

Joint Component Design for the JSCC System Based on DP-LDPC Codes

Sanya Liu¹, Lin Wang¹, *Senior Member, IEEE*, Jun Chen, *Senior Member, IEEE*,
and Shaohua Hong², *Member, IEEE*

Abstract—The joint base matrix B_J of the joint source-channel coding (JSCC) system based on double protograph low-density parity-check (DP-LDPC) codes consists of four components, namely, the source code B_s , the channel code B_c , the type-1 connection edge B_{L1} and the type-2 connection edge B_{L2} , each having a non-negligible influence on the system performance. Different from the traditional component-specific design approach, we propose a joint design and optimization algorithm based on the idea of multi-objective differential evolution (MODE). Specifically, we consider the optimization of the DP-LDPC JSCC system through joint design of three components B_s , B_c , B_{L1} and all four components B_s , B_c , B_{L1} , B_{L2} , respectively. The proposed algorithm has low search complexity due to the reduction in size and element value of base matrices. The joint protograph extrinsic information transfer (JPEXIT) analyses and the simulation results demonstrate that the resulting JSCC system is free from a high error floor, requires fewer number of iterations for reaching the same bit error rate (BER) and achieves significant coding gains as compared to the state-of-the-art. Our DP-LDPC JSCC system is also shown to outperform its separation-based counterpart by a wide margin.

Index Terms—Joint design, JSCC system, DP-LDPC, multi-objective differential evolution (MODE).

I. INTRODUCTION

COMPARED to the conventional source-channel separation paradigm, joint source-channel coding (JSCC) is known to be more efficient in exploiting source/channel characteristics and enable better coordination between source and channel encoders/decoders. As such, JSCC technologies are able to offer significant improvement over their separation-based counterparts in terms of achievable throughput, system complexity, energy efficiency, and end-to-end

latency [1]–[4]. These advantages render JSCC particularly attractive for speech, image, and video transmission [5]–[9]. JSCC has also found applications in many other scenarios (e.g., underwater communications [10]).

There are many approaches to developing JSCC schemes, with apparatus ranging from space-filling curves [10] to deep neural networks [9]. The particular approach adopted in the present work can be traced back to Gallager’s remarkable doctoral dissertation [11]. Specifically, in [11], Gallager proposed a new class of linear block error-correcting codes named low-density parity-check (LDPC) codes, which can be represented by very sparse check matrices [11]. LDPC codes began to attract the attention of the research community in 80s, and were extended with the code graphs introduced by Tanner [12]. However, due to the lack of structure, traditional LDPC codes have high encoding and decoding complexity, which, to a certain extent, limits their application in communication systems. For this reason, significant effort has been devoted to designing more efficient LDPC codes. In 2003, Thorpe proposed a new kind of structured LDPC codes based on a template called protograph (consequently, such codes are called protograph LDPC (P-LDPC) codes). A protograph is a Tanner graph with a relatively small number of nodes, which can be used to construct LDPC codes of arbitrary size and predict the performance of the resulting codes [13]. P-LDPC codes admit efficient encoding and decoding, and are amenable to hardware implementation [14]. Moreover, compared with traditional LDPC codes, P-LDPC codes have superior error correction performance [14], [15].

There has been extensive research on P-LDPC codes, which can be viewed as a subclass of multi-edge type LDPC codes [16]. Divsalar *et al.* proposed methods for constructing P-LDPC codes with low thresholds and linear minimum distance growth (low error floor), and used them to design a series of codes with good performance [14], [15], [17]–[19]. Nguyen *et al.* constructed rate-compatible P-LDPC codes for a wide range of rates under various requirements [20]–[22]. In [23], Uchikawa designed a new family of non-precoded P-LDPC codes with good performance under the circumstances of small decoding iterative number. In addition, large-girth P-LDPC code sequences with block-error thresholds were studied and constructed deterministically [24]. The optimization of P-LDPC codes for non-standard channels was studied in [25]. See also [26], [27] for some most recent work on the applications of P-LDPC codes.

Manuscript received April 3, 2020; accepted May 30, 2020. Date of publication June 11, 2020; date of current version September 16, 2020. This work was supported by the National Natural Science Foundation of China under Grant 61671395 and by Guangdong Natural Science Foundation (No. 2018A030313710). The associate editor coordinating the review of this article and approving it for publication was S. Rini. (*Corresponding author: Lin Wang.*)

Sanya Liu and Lin Wang are with the Department of Information and Communication Engineering, Xiamen University, Xiamen 361005, China (e-mail: sanyaliu1106@gmail.com; wanglin@xmu.edu.cn).

Jun Chen is with the Department of Electrical and Computer Engineering, McMaster University, Hamilton, ON L8S 4L8, Canada (e-mail: junchen@mail.ece.mcmaster.ca).

Shaohua Hong is with the Department of Information and Communication Engineering, Xiamen University, Xiamen 361005, China, and also with Shenzhen Research Institute, Xiamen University, Shenzhen 518057, China (e-mail: hongsh@xmu.edu.cn).

Color versions of one or more of the figures in this article are available online at <http://ieeexplore.ieee.org>.

Digital Object Identifier 10.1109/TCOMM.2020.3001647

0090-6778 © 2020 IEEE. Personal use is permitted, but republication/redistribution requires IEEE permission.
See <https://www.ieee.org/publications/rights/index.html> for more information.

By exploiting the redundant information in source data to perform joint decoding at the decoder end, JSCC is able to achieve significant coding gains compared with separation-based coding. LDPC codes were originally developed for channel coding, and were known to be able to approach the Shannon limit under iterative decoding [28]. In 2010, unstructured regular LDPC codes and irregular LDPC codes were introduced into JSCC and developed to the double LDPC (D-LDPC) system [29]. The double P-LDPC (DP-LDPC) JSCC system [30] is a variant of the D-LDPC system with the traditional LDPC codes replaced by the P-LDPC codes, which have simpler constructions and better code rate extensibility. Simulation results show that the DP-LDPC JSCC system has better performance compared with its D-LDPC counterpart.

A. Related Work and Motivation

Recent years have seen a growing body of literature on the DP-LDPC JSCC system. Firstly, it was found in [30] that the source statistics have a significant impact on the performance of the JSCC system (see [31] and [32] for further discussions). An important observation is that the bit error rate (BER) performance improves along with the decrement of the source entropy [30]–[32]. With this observation in mind, the source PEXIT [33] was proposed to calculate the source decoding threshold, which helped to lower the error floor of source codes for different rates and different source statistics. Secondly, significant amount of research was devoted to optimizing the code design. The channel code was redesigned to improve the waterfall performance of the DP-LDPC system, and the joint protograph extrinsic information transfer (JPEXIT) was put forward to analyze the threshold of the joint base matrix \mathbf{B}_J [34]. The source P-LDPC code was optimized to improve the error-floor performance [35]. In addition, to lower the error floor of the JSCC system, linking edges (i.e., \mathbf{B}_{L2}) were added between the check nodes (CNs) of the channel code and the variable nodes (VNs) of the source code, which was equivalent to increasing the amount of information about the source bits available in the decoding process [36]. The edge connection (\mathbf{B}_{L1} or \mathbf{B}_{L2}) was studied for the DP-LDPC JSCC system in [37], [38]. To fully explore the influence of the first type of connection edge \mathbf{B}_{L1} , an algorithm for searching the optimal \mathbf{B}_{L1} was proposed in [38] to improve the waterfall performance of the system when the source code and the channel code were fixed. The application of the DP-LDPC JSCC system in image transmission has also been studied, and effective schemes have been put forward [39], [40].

There have also been some efforts to perform joint optimization. A JSCC system with improved waterfall performance was designed in [41] by using a source code \mathbf{B}_s and channel code \mathbf{B}_c pair with lower decoding threshold than the classical reference code pairs. In view of the influence of the variable node of degree-2 on the DP-LDPC JSCC system, the source code \mathbf{B}_s or the channel code \mathbf{B}_c with different number of degree-2 VNs was designed to improve the performance of the waterfall area of the system [42]. Note that [41] and [42] only optimize two components in the joint base matrix, and

neglect the influence of two types of connection edges on the DP-LDPC JSCC system.

In summary, the existing works exclusively focus on optimizing one or two components of the the joint base matrix \mathbf{B}_J , and there is no comprehensive method that can handle the optimization of all four components simultaneously. Against this backdrop, the present paper aims to develop a systematic approach to addressing the joint component optimization problem.

B. Contribution

In order to optimize \mathbf{B}_J more efficiently, this paper proposes a new algorithm for joint component design based on the idea of multi-objective differential evolution (MODE) [43]. The proposed algorithm takes into account various influencing factors simultaneously in system design, such as source distribution, code rate, code length, row weight, column weight, and even the range of specific element value of the code. Specifically, we design \mathbf{B}_J by jointly optimizing three components \mathbf{B}_s , \mathbf{B}_c , \mathbf{B}_{L1} and all four components \mathbf{B}_s , \mathbf{B}_c , \mathbf{B}_{L1} , \mathbf{B}_{L2} , respectively, to avoid high error floor and achieve lower decoding threshold simultaneously. It is shown that the resulting JSCC system significantly outperforms its separation-based counterpart in terms of energy efficiency. Moreover, the designed base matrices have smaller size and element values, which effectively reduces the search complexity and facilitates the encoding/decoding process. As a consequence, our system achieves lower end-to-end latency compared with the state-of-the-art, rendering it more favorable for delay-sensitive applications.

The rest of this paper is organized as follows. Section II describes the JSCC system model and related notations. Section III presents a new algorithm for optimizing the joint base matrix together with two application examples. The simulation and comparison results are shown in Section IV. Finally, we conclude the paper in Section V.

II. SYSTEM MODEL AND RELATED NOTATIONS

For the sake of clarity, the block diagram of the DP-LDPC JSCC system in this paper is shown in Fig. 1. The system formed by the serial connection of two P-LDPC codes where the outer and the inner codes perform source compression and channel coding, respectively, at the sending end. The source \mathbf{s} is first compressed by the outer P-LDPC code into sequence \mathbf{b} at the source encoder. This is followed by channel coding with the inner P-LDPC code. Then, binary phase shift keying (BPSK) is adopted to modulate the codeword \mathbf{c} before transmission over the additive white Gaussian noise (AWGN) channel. Finally, at the decoder, the source sequence $\hat{\mathbf{s}}$ is reconstructed by the joint source-channel (JSC) decoder using the joint belief propagation (BP) algorithm.

Fig.2 depicts the Tanner graph of the DP-LDPC system. The black squares represent the CNs of the source code and the channel code. The black, white and gray circles indicate the source VNs, the punctured channel VNs and the transmitted channel VNs, respectively. The source P-LDPC (left) is represented by the base matrix \mathbf{B}_s of size $m_s \times n_s$; its VNs and CNs specify the source output and the compressed

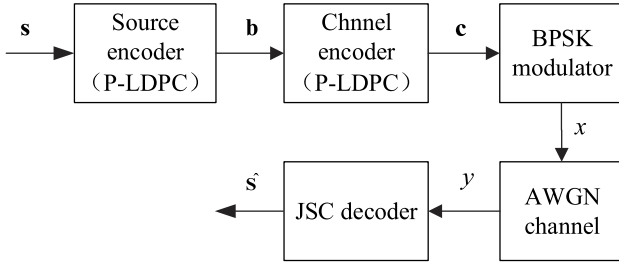


Fig. 1. The block diagram of the DP-LDPC JSCC system.

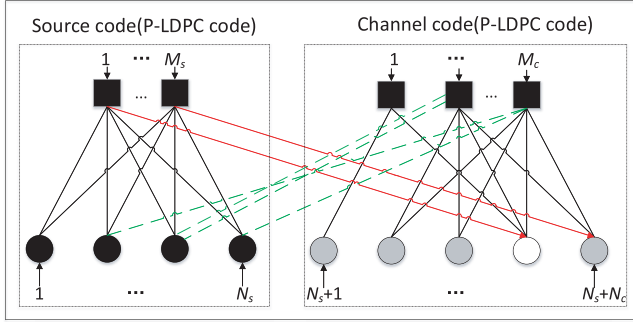


Fig. 2. The Tanner graph of the DP-LDPC JSCC system with two types of edge connections.

source sequence, respectively. The right side of the figure is the channel P-LDPC code, which is represented by the base matrix \mathbf{B}_c of size $m_c \times n_c$. Type-1 link base matrix \mathbf{B}_{L1} , which is of dimension $m_s \times n_c$, specifies the connections between the CNs of the source code and the VNs of the channel code. Type-2 link base matrix \mathbf{B}_{L2} , which is of dimension $m_c \times n_s$, specifies the connections between the VNs of source code and the CNs of channel code. The whole Tanner graph can be represented by a single joint base matrix defined as

$$\mathbf{B}_J = \begin{bmatrix} \mathbf{B}_s & \mathbf{B}_{L1} \\ \mathbf{B}_{L2} & \mathbf{B}_c \end{bmatrix}, \quad (1)$$

where the dimension of the joint base matrix \mathbf{B}_J is $(m_s + m_c) \times (n_s + n_c)$. Note that the output compressed bit sequence of the source code serves as the input information sequence of the channel code. So the sizes of \mathbf{B}_s and \mathbf{B}_c in \mathbf{B}_J must obey the matching condition:

$$n_c - m_c = m_s. \quad (2)$$

The minimum expansion is performed using the progressive edge growth (PEG) algorithm [44] to ensure that the matching condition is satisfied (if the original base matrix does not meet this condition).

The PEG algorithm is then employed to obtain the corresponding joint parity-check matrix \mathbf{H}_J of dimension $(M_s + M_c) \times (N_s + N_c)$ by “copy-and-permute” operation on the joint base matrix \mathbf{B}_J . The matrix is given by

$$\mathbf{H}_J = \begin{bmatrix} \mathbf{H}_s & \mathbf{H}_{L1} \\ \mathbf{H}_{L2} & \mathbf{H}_c \end{bmatrix}, \quad (3)$$

where \mathbf{H}_s with size $M_s \times N_s$ is the source code parity-check matrix, \mathbf{H}_c with size $M_c \times N_c$ is the channel code parity-check matrix, \mathbf{H}_{L1} with size $M_s \times N_c$ specifies connections between

the CNs of source code and the VNs of channel code, and \mathbf{H}_{L2} with size $M_c \times N_s$ specifies connections between the VNs of source code and the CNs of channel code.

Since each CN of the source code is connected to a single VN of the channel code forming the systematic part of the channel codeword, \mathbf{B}_{L1} and the corresponding \mathbf{H}_{L1} can be written in the form of $[\mathbf{0}, \mathbf{I}]$, where $\mathbf{0}$ and \mathbf{I} denote the zero matrix (meaning no connection) and the identity matrix, respectively. Therefore, \mathbf{H}_J can be expressed as:

$$\mathbf{H}_J = \left[\begin{array}{c|c|c} \mathbf{H}_s & \mathbf{0} & \mathbf{I} \\ \hline \mathbf{H}_{L2} & & \mathbf{H}_c \end{array} \right]. \quad (4)$$

In order to understand the encoding and decoding process of the system, the two parts of the encoder and the decoder will be described in detail.

A. Encoder

Let $\mathbf{s} = (s_1, s_2, \dots, s_n) \in \{0, 1\}^n$ be a binary i.i.d. source. The source entropy is given as follows

$$H_p = -p \log_2 p - (1-p) \log_2 (1-p), \quad (5)$$

where p is the probability of “1” and $p \neq 0.5$.

The encoding process of the DP-LDPC JSCC system consists of the following steps:

(1) The source sequence \mathbf{s} is first compressed by the source encoder parity-check matrix matrix \mathbf{H}_s . Compute $\mathbf{b} = \mathbf{s} \cdot \mathbf{H}_s^T$, where \mathbf{b} is the compressed bit sequence. Note that this step is the source coding step.

(2) Combine \mathbf{s}_p and \mathbf{b} as $[\mathbf{s}_p, \mathbf{b}]$, i.e., the horizontal cascade of sequences \mathbf{s}_p and \mathbf{b} , where \mathbf{s}_p is the part of \mathbf{s} connected by the CNs of the channel code.

(3) The codeword is obtained by $\mathbf{c} = [\mathbf{s}_p, \mathbf{b}] \cdot \mathbf{G}_{L2c} = [\mathbf{s}_p, \mathbf{b}] \cdot [\mathbf{I}, \mathbf{P}^T] = [[\mathbf{s}_p, \mathbf{b}] \cdot \mathbf{I}, [\mathbf{s}_p, \mathbf{b}] \cdot \mathbf{P}^T] = [\mathbf{s}_p, \mathbf{b}, \mathbf{p}]$, where \mathbf{G}_{L2c} is an $(N_s + N_c - M_c) \times (N_s + N_c)$ generator matrix whose parity-check matrix is given by the horizontal cascade of the matrices \mathbf{H}_{L2} and \mathbf{H}_c . Then $\mathbf{G}_{L2c} \cdot [\mathbf{H}_{L2}, \mathbf{H}_c]^T = \mathbf{0}$ and $\mathbf{G}_{L2c} = [\mathbf{I}, \mathbf{P}^T]$. In addition, $\mathbf{p} = [\mathbf{s}_p, \mathbf{b}] \cdot \mathbf{P}^T$. Note that this step is the channel coding step.

(4) Transmit \mathbf{c} after puncturing \mathbf{s}_p . If the channel code is a punctured P-LDPC code, the corresponding parity bits are punctured before transmitting the codeword.

There are two special cases. In one case, the \mathbf{s}_p is $\mathbf{0}$, then the corresponding type-2 link base matrix \mathbf{B}_{L2} is a zero matrix. In the other case, $\mathbf{s}_p = \mathbf{s}$, then the corresponding \mathbf{B}_{L2} is a full rank matrix, which establishes the connections of the CNs of \mathbf{B}_c to all the VNs of \mathbf{B}_s . In the overall design and optimization, we will treat zero and non-zero \mathbf{B}_{L2} separately.

B. Decoder

The joint source and channel (JSC) decoder of the DP-LDPC JSCC system implements the BP algorithm with the goal of producing a source reconstruction $\hat{\mathbf{s}}$. Specifically, the JSC decoder outputs $\hat{\mathbf{c}} = [\hat{\mathbf{s}}_{1-p}, \hat{\mathbf{s}}_p, \hat{\mathbf{b}}, \hat{\mathbf{p}}]$ that satisfies $\hat{\mathbf{c}} \cdot \mathbf{H}_J^T = \mathbf{0}$, where $[\hat{\mathbf{s}}_p, \hat{\mathbf{b}}, \hat{\mathbf{p}}]$ is the channel codeword recovered through decoding, and $\hat{\mathbf{s}} = [\hat{\mathbf{s}}_{1-p}, \hat{\mathbf{s}}_p]$ is a reconstruction of source sequence $\mathbf{s} = [\mathbf{s}_{1-p}, \mathbf{s}_p]$ with \mathbf{s}_{1-p} denoting the residual part of information bits that are not connected in \mathbf{s} .

Let L_v^s and L_v^c be the initial log-likelihood ratios (LLRs) of the source code VNs and the channel code VNs, respectively. We use $L_{v,c}^{it}$ ($L_{c,v}^{it}$) to represent the LLR passed from the v -th VN (c -th CN) to the c -th CN (v -th VN) in the it -th iteration. The decoding process can be expressed as follows:

(1) Initialization of L_v^s and L_v^c :

$$L_v^s = \ln \frac{1-p}{p}, \quad v = 1, \dots, N_s, \quad (6)$$

$$L_v^c = \ln \frac{\Pr(x_v = +1|y_v)}{\Pr(x_v = -1|y_v)} = \frac{2y_v}{\sigma^2}, \quad v = N_s + 1, \dots, N_s + N_c, \quad (7)$$

where $\Pr(\cdot)$ denotes the probability function, $y_v = x_v + n_v$ denotes the v -th received signal transmitted through the channel, $x_v \in \{-1, +1\}$ is the signal modulated by BPSK with the mapping rule $0 \rightarrow +1$ and $1 \rightarrow -1$, $n_v \sim (0, \sigma^2)$ is the variance of the Gaussian channel noise. If the channel VN is punctured, the received bit $y_v = 0$ and consequently its initial LLR value is 0.

(2) The LLRs passed from the VNs to the CNs:

$$L_{v,c}^{it} = L_v^s + \sum_{c' \neq c} L_{c',v}^{it-1}, \quad v = 1, \dots, N_s, \quad (8)$$

$$L_{v,c}^{it} = L_v^c + \sum_{c' \neq c} L_{c',v}^{it-1}, \quad v = N_s + 1, \dots, N_s + N_c, \quad (9)$$

where $c' \neq c$ denotes all CNs connected to the v -th VN excluding the c -th CN.

(3) The LLRs passed from the CNs to the VNs:

$$\tanh\left(\frac{L_{c,v}^{it}}{2}\right) = \prod_{v' \neq v} \tanh\left(\frac{L_{v',c}^{it-1}}{2}\right), \quad c = 1, \dots, M_s + M_c, \quad (10)$$

where $v' \neq v$ denotes all VNs connected to the c -th CN excluding the v -th VN.

(4) The final posterior LLRs of the source P-LDPC code VNs when the set maximum number of iterations it_{max} is reached:

$$L(s_v) = L_v^s + \sum_c L_{c,v}^{it_{max}}, \quad v = 1, \dots, N_s. \quad (11)$$

(5) Reconstruction of the source bits:

$$\hat{s}_v = \begin{cases} 0, & L(s_v) \geq 0 \\ 1, & L(s_v) < 0. \end{cases} \quad (12)$$

In summary, each iteration consists of two parts. In the first half iteration the LLRs are passed from the VNs to the CNs while in the second half iteration the LLRs are passed from the CNs to the VNs. When the maximum number of iterations is reached, the joint decoding process stops, and the source bits are estimated according to the final posterior LLRs ($L(s_v)$) of the source P-LDPC code VNs.

III. DESIGN METHOD AND OPTIMIZATION PROCESS

In this paper, an algorithm based on MODE is proposed for the design of joint base matrix by optimizing all components simultaneously. The algorithm aims to not only improve the performance in the waterfall area but also reduce the error floor. It takes the source threshold, joint source channel code threshold and the factors affecting the properties of the P-LDPC code as the control variables and constraints. Binomial crossover and difference vector mutation are used to automatically adjust the parameters of the differential evolution strategy. The feasibility and effectiveness of the proposed design and optimization algorithm is verified by the experimental results.

In this section, the search method—MODE—used in our code design and optimization is described. Then the design procedure and the new P-LDPC code construction examples are presented.

A. Properties and Corresponding Influencing Factors in \mathbf{B}_J

The attributes and the associated influencing factors of a good P-LDPC code are summarized as follows.

(i) Low iterative decoding threshold

a. According to [14], a good protograph should contain one or more degree-1 VNs, one very high degree VN and several degree-2 VNs. Specifically, degree-1 VNs (accumulators) serve as pre-coders to improve the iterative decoding threshold; they do not affect the growth of minimum distance with codeword length. Including one very high degree VN and several degree-2 VNs can also improve the iterative decoding threshold.

b. If puncturing is required, search for the optimal puncturing pattern that results in the lowest threshold.

(ii) Linear minimum distance growth

a. The number of degree-2 VNs in \mathbf{B}_c is at most $m_c - m_p - 1$, where m_p is the number of pre-coders.

b. The number of degree-2 VNs in \mathbf{B}_J is at most $m_J - m_p - 1$, where $m_J = m_s + m_c$ is the number of CNs of \mathbf{B}_J .

c. \mathbf{B}_s , \mathbf{B}_c and \mathbf{B}_J do not contain CNs of degree 1.

(iii) Computational complexity and searching complexity in the optimization process

Let K denote the maximum value of the elements in the matrix. The larger the K value and the sizes of base matrices, the larger the search space becomes, which leads to higher computational complexity and searching complexity in the optimization process [14], [20].

B. The Objective Function

The MODE algorithm aims to solve the so-called multi-objective optimization problem (MOP), for which multiple optimization objective functions are simultaneously minimized or maximized subject to a series of equality and inequality constraints. The joint design and optimization problem considered in this work is a MOP with two optimization objective functions, which can be formulated as follows:

$$\min_{\mathbf{B}_J \in R} [Th(\mathbf{B}_J), -STh(\mathbf{B}_J)] \quad (13)$$

$$s.t. \quad R \quad (14)$$

where $Th(\mathbf{B}_J)$ and $STh(\mathbf{B}_J)$ are two optimization objective functions, which are the decoding threshold (calculated by the JPEXIT) and the source threshold (calculated by the source PEXIT) of \mathbf{B}_J . R is the feasible domain that meets conditions (i) ~ (iii) in Section III(A).

In addition, the following constraints are also imposed on $Th(\mathbf{B}_J)$ and $STh(\mathbf{B}_J)$:

(1) $Th-min < Th(\mathbf{B}_J) < Th-max$, where $Th-min$ is the Shannon limit, and $Th-max$ is the decoding threshold of the classic codes to be surpassed.

(2) $STh(\mathbf{B}_J) > p$, which ensures that the designed \mathbf{B}_J can meet the requirement of BER reaching 10^{-6} .

C. The Joint Design and Optimization Algorithm

The Differential Evolution (DE) algorithm [45] is a group-based random search algorithm. This paper extends the DE algorithm to solve the multi-objective optimization problem. The optimization variables are expressed as four-component basis matrices in the evolutionary population. The algorithm starts the exploration of the search space by randomly selecting the initial candidate solutions within the boundaries. The flow chart of the proposed joint design and optimization algorithm is shown in Fig.3. And the specific operation steps are described in detail as follows.

Input:

(i) The MOP is optimized with two objectives: $Th(\mathbf{B}_J)$ and $STh(\mathbf{B}_J)$.

(ii) The feasible domain of search space R : conditions (i) ~ (iii) in Section III(A).

(iii) Initialization of parameters:

a. The source statistic p , the source code rate R_s , the channel code rate R_c , the base matrices sizes m_s, n_s, m_c, n_c , the preset maximum and minimum values $Th-min$ and $Th-max$ are given.

b. Select the size of candidate matrices per generation NP (the selection range of low-dimensional simple problems is [15, 35] and that of high-dimensional complex problems is [30, 50]), the maximum evolution generation $Gmax$, crossover factor $CR \sim [0, 1]$ (the selection intervals are [0.6, 0.8] and [0.1, 0.5] for single-peak function and complex multi-peak function, respectively), scaling factor $F \sim [0, 2]$ (with the recommendation of interval [0.5, 1]). See [43] for the selection of these parameters. The maximum value of the element in the base matrix is K .

step 1: Generate initial base matrices $\mathbf{B}_{J(pop)}^1$ ($\mathbf{B}_{J(pop)}^G$) denotes the pop -th matrix in the G -th generation, $pop=1, 2, \dots, NP$, $G=1, 2, \dots, Gmax$). $\mathbf{B}_{J(pop)}^1$ consists of the initial base matrices of four components $\mathbf{B}_{s(pop)}^1, \mathbf{B}_{c(pop)}^1, \mathbf{B}_{L1(pop)}^1$ and $\mathbf{B}_{L2(pop)}^1$. $\mathbf{B}_{J(pop)}^1$ ($pop > 1$) is generated by replacing the element in $\mathbf{B}_{J(pop-1)}^1$, except fixed elements, with values randomly chosen from 0, 1, ..., K . Each joint base matrix generated by this process satisfies constraints (i) ~ (iii) in Section III(A).

step 2: Calculate the fitness values $Th(\cdot)$ and $STh(\cdot)$ of each joint base matrix in the initial generation.

step 3: Perform differential operations (i.e., mutation and crossover) on the joint base matrices in the parent-generation to produce the child-generation joint base matrices, and calculate the fitness values of the corresponding joint base matrices.

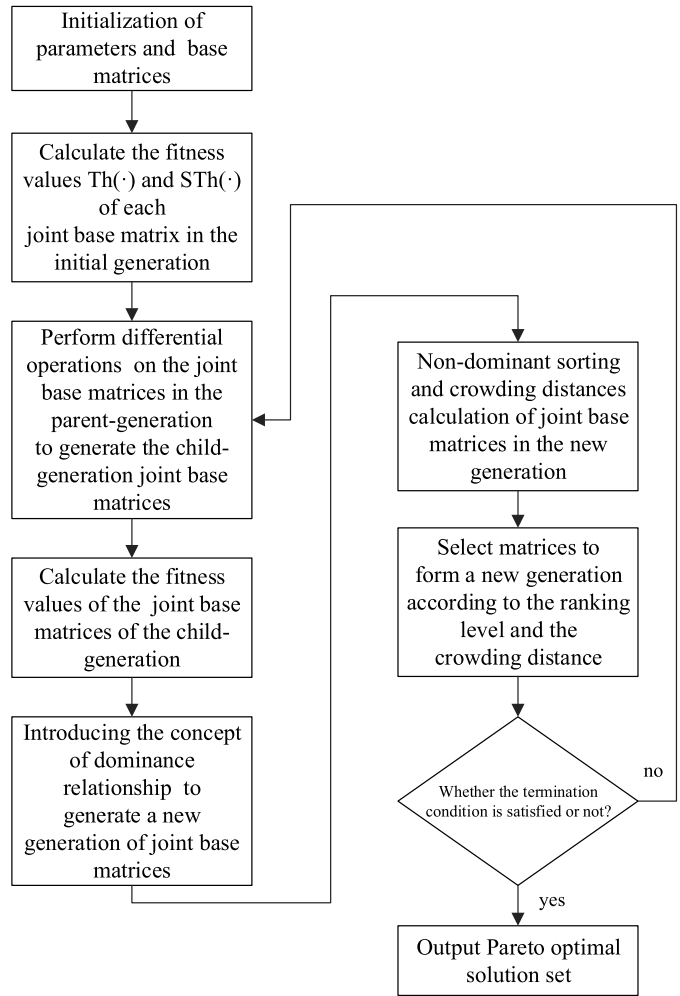


Fig. 3. The flow chart of the proposed joint design and optimization algorithm.

step 4: The child-generation joint base matrices and the parent-generation joint base matrices obtained by the differential operation will be compared based on the concept of dominance relationship to generate a new generation of joint base matrices.

a. When the matrix in the child-generation dominates the matrix of the parent-generation, the parent-generation is abandoned and replaced by the former.

b. When the matrix in the parent-generation dominates the matrix of the child-generation, the latter is abandoned, while the former remains unchanged.

c. When the matrix in the parent-generation and the matrix in the child-generation do not dominate each other, then the latter is added to the current generation.

step 5: The size of the new generation obtained in step 4 is between NP and $2 \times NP$, so it is necessary to perform a cut-off operation to construct a next generation of joint base matrices. To perform so-called cut-off, we first rank the individuals non-dominantly and calculate their crowding distance, then select the top NP joint base matrices to form a new generation according to the ranking level and the crowding distance.

Step 6: Preset a maximum number of evolution iterations $Gmax$. If the maximum number of iterations is not reached, let

Algorithm 1 The Joint Design and Optimization Algorithm

-
- 1: Set $p, R_s, R_c, m_s, n_s, m_c, n_c, Th\text{-min}, Th\text{-max}, NP, Gmax, CR, F,$ and K ;
 - 2: **for** $pop=1, 2, \dots, NP$ **do**
 - 3: Generate initial base matrices $\mathbf{B}_{s(pop)}^1, \mathbf{B}_{c(pop)}^1, \mathbf{B}_{L1(pop)}^1,$ and $\mathbf{B}_{L2(pop)}^1$ according to required properties (see Section III(A));
 - 4: Combine them to form the initial joint basis matrix $\mathbf{B}_{J(pop)}^1$;
 - 5: Calculate the fitness values $Th(\mathbf{B}_{J(pop)}^1)$ and $STh(\mathbf{B}_{J(pop)}^1)$;
 - 6: **end for**
 - 7: **for** $G=2, 3, \dots, Gmax$ **do**
 - 8: **for** $pop=1, 2, \dots, NP$ **do**
 - 9: Perform differential operations on $\mathbf{B}_{J(pop)}^{G-1}$ to produce $\mathbf{B}_{J(pop)}^G$;
 - 10: Calculate the fitness values $Th(\mathbf{B}_{J(pop)}^G)$ and $STh(\mathbf{B}_{J(pop)}^G)$;
 - 11: **if** $\mathbf{B}_{J(pop)}^G$ dominates $\mathbf{B}_{J(pop)}^{G-1}$
 - 12: $\mathbf{B}_{J(pop)}^G \leftarrow \mathbf{B}_{J(pop)}^G$;
 - 13: **else**
 - 14: **if** $\mathbf{B}_{J(pop)}^{G-1}$ dominates $\mathbf{B}_{J(pop)}^G$
 - 15: $\mathbf{B}_{J(pop)}^G \leftarrow \mathbf{B}_{J(pop)}^{G-1}$;
 - 16: **else**
 - 17: $\mathbf{B}_{J(pop)}^G \leftarrow \mathbf{B}_{J(pop)}^{G-1}$;
 - 18: $\mathbf{B}_{J(NP+pop)}^G \leftarrow \mathbf{B}_{J(pop)}^G$;
 - 19: **end if**
 - 20: **end if**
 - 21: **end for**
 - 22: **for** $pop=1, 2, \dots, NP+pop$ **do**
 - 23: Non-dominant sorting and crowding distances calculation of $\mathbf{B}_{J(pop)}^G$;
 - 24: **end for**
 - 25: select the top NP joint base matrices to form a new $\mathbf{B}_{J(pop)}^G$;
 - 26: **end for**
 - 27: **output:** $\mathbf{B}_J^{opti}, Th(\mathbf{B}_J^{opti})$.
-

the number of generation $G = G + 1$ and return the operation to step 3. Otherwise, the Pareto optimal solution set of the problem is output and the operation is terminated.

See **Algorithm 1** for the pseudo-code of the joint design and optimization algorithm, where \mathbf{B}_J^{opti} represents the optimal joint base matrix obtained through the proposed algorithm.

D. Design and Optimization Example 1

For the first example, we consider the joint design and optimization problem with type-2 connection edges excluded, that is, $\mathbf{B}_{L2} = 0$.

1) *Initialization of Parameters:* To facilitate the comparisons with the optimal codes designed in the literature [41] and [42], the source code and the channel code with rate 1/2 are designed for the i.i.d. Bernoulli source with $p = 0.04$. The sizes of \mathbf{B}_s and \mathbf{B}_c are chosen to be 2×4 and 3×5 (i.e., one VN needs to be punched), while the sizes of

two types of connection matrices $\mathbf{B}_{L1}, \mathbf{B}_{L2}$ and the joint base matrix \mathbf{B}_J are $2 \times 5, 3 \times 4$, and 5×9 , respectively. Moreover, we set the size of candidate matrices per generation $NP = 35$, maximum evolution generation $Gmax = 500$, cross factor $CR = 0.8$, scaling factor $F = 0.5$, and the maximum element value $K = 3$.

2) *Initialization of the Joint Base Matrix:* Taking into account the required properties of a good P-LDPC code (see Section III(A)), the system characteristics and the fact that \mathbf{B}_{L1} is not connected to the pre-coder (degree-1 part or a rate-1 accumulation) [20] column, the initial joint base matrix is set as

$$\mathbf{B}_{J(1)}^1 = \begin{bmatrix} 1 & 1 & 1 & 1 & 0 & 1 & 0 & 0 & 0 \\ 1 & 1 & 1 & 1 & 0 & 0 & 1 & 0 & 0 \\ \hline & & & & 1 & 1 & 1 & 1 & 0 \\ & \mathbf{0} & & & 0 & 1 & 1 & 1 & 1 \\ & & & & 0 & 1 & 1 & 1 & 1 \end{bmatrix}, \quad (15)$$

where the elements in the last column of \mathbf{B}_s , the first and the last columns of $\mathbf{B}_c, \mathbf{B}_{L1}$, and \mathbf{B}_{L2} are fixed. If more than one VN with the highest degree exist, one of them will be chosen arbitrarily and punctured. Another point to note is that \mathbf{B}_{L1} is not linked with the pre-coder because the performance of the DP-LDPC JSCC system is unstable otherwise.

The optimized joint base matrix obtained by the proposed joint design and optimization algorithm is as follows:

$$\mathbf{B}_J^{opti.1} = \begin{bmatrix} 2 & 2 & 1 & 1 & 0 & 1 & 0 & 0 & 0 \\ 1 & 1 & 2 & 1 & 0 & 0 & 1 & 0 & 0 \\ \hline & & & & 1 & 2 & 2 & 1 & 0 \\ & \mathbf{0} & & & 0 & 1 & 1 & 1 & 1 \\ & & & & 0 & 0 & 2 & 1 & 1 \end{bmatrix}, \quad (16)$$

where, for \mathbf{B}_c , the third VN is punctured.

In addition, since increasing the code length tends to reduce the error floor to a certain extent, we consider a relaxed version of the optimization problem by removing a of condition (ii) in Section III(A), which yields the following joint base matrix:

$$\mathbf{B}_J^{opti.2} = \begin{bmatrix} 1 & 2 & 1 & 1 & 0 & 1 & 0 & 0 & 0 \\ 2 & 1 & 2 & 1 & 0 & 0 & 1 & 0 & 0 \\ \hline & & & & 1 & 1 & 3 & 0 & 0 \\ & \mathbf{0} & & & 0 & 0 & 2 & 1 & 1 \\ & & & & 0 & 1 & 1 & 1 & 1 \end{bmatrix}, \quad (17)$$

where the third VN of \mathbf{B}_c is punctured. Note that the joint base matrix designed under the relaxed conditions can be regarded as a design for long codewords, and the joint base matrix designed under the unrelaxed conditions corresponding Equation (16) can be applied to short-to-moderate-length codewords.

For convenience of description, the joint base matrix corresponding to the code pairs $(\mathbf{B}_{s1}, \mathbf{B}_{c1})$ optimized for long codewords in [41] is denoted as $\mathbf{B}_{J,1}$ [41]. The joint base matrix corresponding to the code pairs $(\mathbf{B}_{s3}, \mathbf{B}_{c1})$ optimized for short-to-moderate-length codewords is denoted as $\mathbf{B}_{J,3}$ [41]. The optimal joint base matrix corresponding to Equation (14) optimized for short-to-moderate-length codewords in [42] is denoted as \mathbf{B}_J [42]. Table I lists the thresholds of the five joint base matrices. It can be seen that the coding gains of the optimized design under unrelaxed conditions relative to

TABLE I

DECODING THRESHOLDS OF THE FIVE JOINT BASE MATRICES ($\mathbf{B}_{L2} = 0$)

Type	Equation	Threshold
unrelaxed	$\mathbf{B}_J^{opti_1}$	-2.288 dB
for short-to-moderate-length codewords	\mathbf{B}_{J_3} [41]	-1.738 dB
for short-to-moderate-length codewords	\mathbf{B}_J [42]	-2.128 dB
relaxed	$\mathbf{B}_J^{opti_2}$	-2.388 dB
for long codewords	\mathbf{B}_{J_1} [41]	-2.129 dB

the previous solutions for short-to-moderate-length codewords in [41] and [42] are 0.55 dB and 0.16 dB, respectively; moreover, the optimized design under relaxed conditions achieves 0.26 dB gain over the previous solution for long codewords in [41].

E. Design and Optimization Example 2

For the second example, we consider joint design and optimization of all four components, that is to say, the type-2 connection edges are also taken into account (i.e., $\mathbf{B}_{L2} \neq 0$).

Initialization of parameters: The same as in Example 1.

Initialization of the joint base matrix: It is also the same as Example 1. In addition, \mathbf{B}_{L2} is not connected to the pre-coder for the same reason as \mathbf{B}_{L1} . So the initial joint base matrix is given by

$$\mathbf{B}_{J(1)}^1 = \begin{bmatrix} 1 & 1 & 1 & 1 & 0 & 1 & 0 & 0 & 0 \\ 1 & 1 & 1 & 1 & 0 & 0 & 1 & 0 & 0 \\ 0 & 0 & 0 & 0 & 1 & 1 & 1 & 1 & 0 \\ 1 & 1 & 1 & 0 & 0 & 1 & 1 & 1 & 1 \\ 1 & 1 & 1 & 0 & 0 & 1 & 1 & 1 & 1 \end{bmatrix}, \quad (18)$$

where the elements in the last column of \mathbf{B}_s , the first and the last columns of \mathbf{B}_c , \mathbf{B}_{L1} , the first row and the last column of \mathbf{B}_{L2} are fixed. Likewise, the VN with the highest degree in \mathbf{B}_c is punctured and one of them will be chosen randomly and punctured if there are more than one VNs with the highest degree.

The joint base matrix produced by the proposed joint design and optimization algorithm is given as follows:

$$\mathbf{B}_{J^{opti_3}} = \begin{bmatrix} 3 & 1 & 1 & 1 & 0 & 1 & 0 & 0 & 0 \\ 3 & 1 & 1 & 1 & 0 & 0 & 1 & 0 & 0 \\ 0 & 0 & 0 & 0 & 1 & 2 & 1 & 1 & 0 \\ 0 & 0 & 1 & 0 & 0 & 1 & 1 & 1 & 1 \\ 0 & 0 & 0 & 0 & 0 & 1 & 1 & 1 & 1 \end{bmatrix}, \quad (19)$$

where the second VN of \mathbf{B}_c is punctured.

On the other hand, with a in condition (ii) removed, the proposed algorithm yields the following joint basis matrix:

$$\mathbf{B}_{J^{opti_4}} = \begin{bmatrix} 3 & 2 & 2 & 1 & 0 & 1 & 0 & 0 & 0 \\ 3 & 1 & 1 & 1 & 0 & 0 & 1 & 0 & 0 \\ 0 & 0 & 0 & 0 & 1 & 1 & 2 & 0 & 0 \\ 3 & 0 & 0 & 0 & 0 & 0 & 2 & 1 & 1 \\ 3 & 0 & 0 & 0 & 0 & 1 & 1 & 1 & 1 \end{bmatrix}, \quad (20)$$

where the third VN of \mathbf{B}_c is punctured.

Table II lists the thresholds of the five joint base matrices. It can be seen that the coding gains of the optimized design under unrelaxed conditions relative to the previous solutions for short-to-moderate-length codewords in [41]

TABLE II

DECODING THRESHOLDS OF THE FIVE JOINT BASE MATRICES ($\mathbf{B}_{L2} \neq 0$)

Type	Equation	Threshold
unrelaxed	$\mathbf{B}_J^{opti_3}$	-2.276 dB
for short-to-moderate-length codewords	\mathbf{B}_{J_3} [41]	-1.738 dB
for short-to-moderate-length codewords	\mathbf{B}_J [42]	-2.128 dB
relaxed	$\mathbf{B}_J^{opti_4}$	-2.577 dB
for long codewords	\mathbf{B}_{J_1} [41]	-2.129 dB

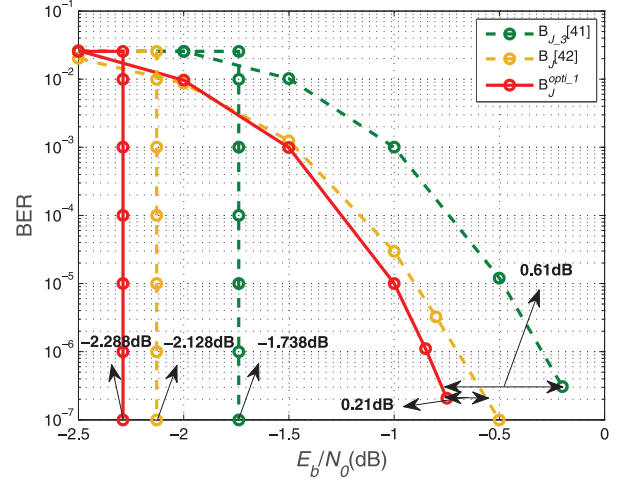


Fig. 4. BER simulation results of the JSCC system based on the proposed joint design and optimization algorithm (under unrelaxed conditions for $\mathbf{B}_{L2} = 0$) and the schemes in [41], [42] at $N = 3200$.

and [42] are about 0.54 dB and 0.15 dB, respectively; moreover, the optimized design under relaxed conditions achieves about 0.45 dB gain over the previous solution for long codewords [41].

IV. SIMULATION RESULTS AND DISCUSSION

Extensive experiments (see Fig. 4 ~ Fig. 13) are carried out to verify the effectiveness of the proposed algorithm. In the first eight groups of experiments, the parity-check matrices are obtained by the PEG algorithm and the maximum number of iterations per frame is 200. The simulation is terminated when there are 1000 frame errors at each SNR value.

In particular, Fig. 4 and Fig. 6 show the BER simulation results of the joint base matrices $\mathbf{B}_J^{opti_1}$ and $\mathbf{B}_J^{opti_3}$ which are optimized under unrelaxed conditions for $\mathbf{B}_{L2} = 0$ and $\mathbf{B}_{L2} \neq 0$, respectively. It can be seen that they outperform \mathbf{B}_{J_3} [41] designed in [41] for short-to-moderate-length codewords ($N = 3200$) by about 0.61 dB and 0.62 dB at $\text{BER} = 10^{-7}$, respectively, and outperform \mathbf{B}_J [42] designed in [42] by about 0.21 dB and 0.20 dB at $\text{BER} = 10^{-7}$, respectively. In addition, it can also be seen that there is still about 1.6 dB optimization space to the threshold for short-to-moderate-length codewords.

Fig. 5 and Fig. 7 plot the simulation BER results of the joint base matrices $\mathbf{B}_J^{opti_2}$ and $\mathbf{B}_J^{opti_4}$ which are optimized under relaxed conditions for $\mathbf{B}_{L2} = 0$ and $\mathbf{B}_{L2} \neq 0$, respectively. It is observed that when $\text{BER} = 10^{-7}$, $\mathbf{B}_J^{opti_2}$ achieves about 0.30 dB gain compared with \mathbf{B}_{J_1} [41] designed in [41] for

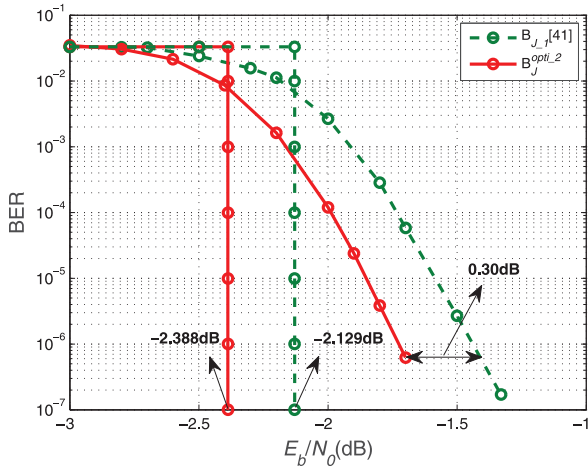


Fig. 5. BER simulation results of the JSCC system based on the proposed joint design and optimization algorithm (under relaxed conditions for $B_{L2} = 0$) and the scheme in [41] at $N = 12800$.

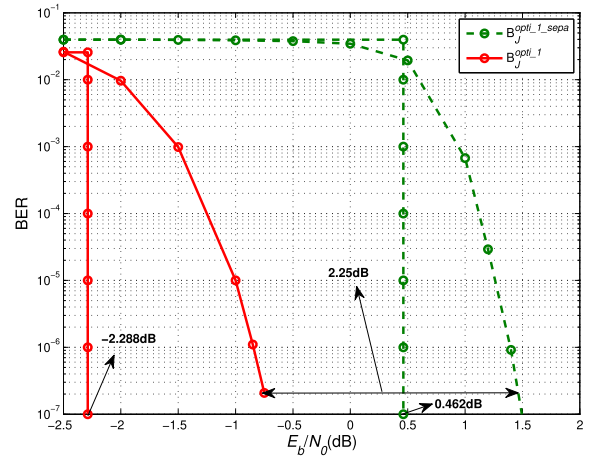


Fig. 8. BER simulation results of the JSCC system based on the proposed joint design and optimization algorithm and its separation-based counterpart at $N = 3200$.

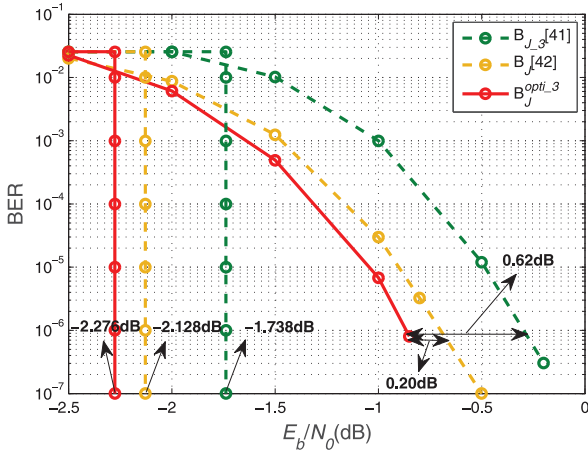


Fig. 6. BER simulation results of the JSCC system based the proposed joint design and optimization algorithm (under unrelaxed conditions for $B_{L2} \neq 0$) and the schemes in [41], [42] at $N = 3200$.

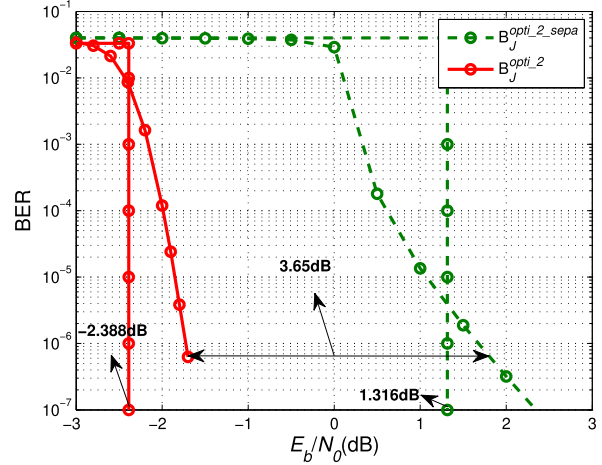


Fig. 9. BER simulation results of the JSCC system based on the proposed joint design and optimization algorithm and its separation-based counterpart at $N = 12800$.

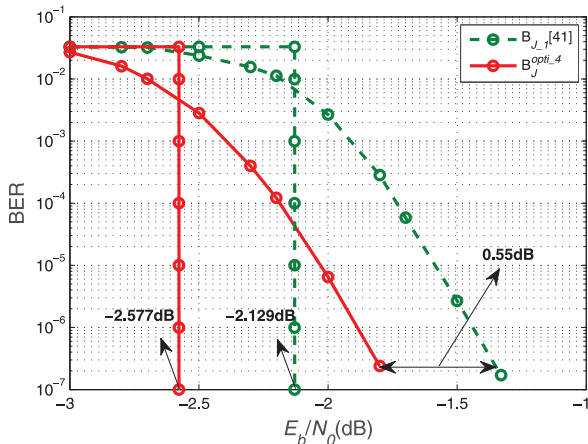


Fig. 7. BER simulation results of the JSCC system based on the proposed joint design and optimization algorithm (under relaxed conditions for $B_{L2} \neq 0$) and the scheme in [41] at $N = 12800$.

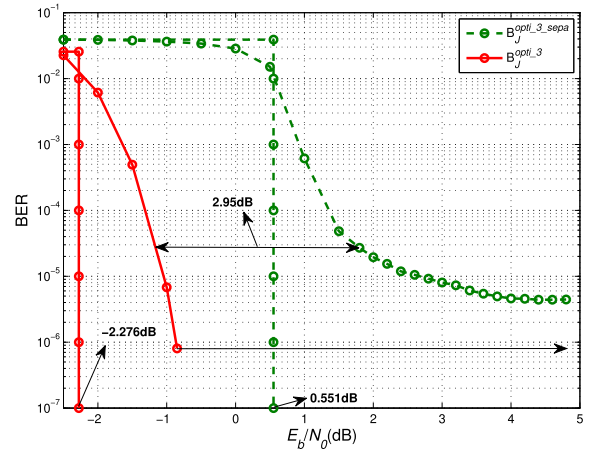


Fig. 10. BER simulation results of the JSCC system based on the proposed joint design and optimization algorithm and its separation-based counterpart at $N = 3200$.

long codewords ($N = 12800$) and $B_J^{opti_4}$ outperforms it by about 0.55 dB. For long codewords, there is still about 0.7 dB optimization space to the threshold.

The comparison between the BER results of our JSCC system (solid lines) and its separation-based counterpart (dashed lines) is depicted in Fig. 8 ~ Fig. 11. It can be seen

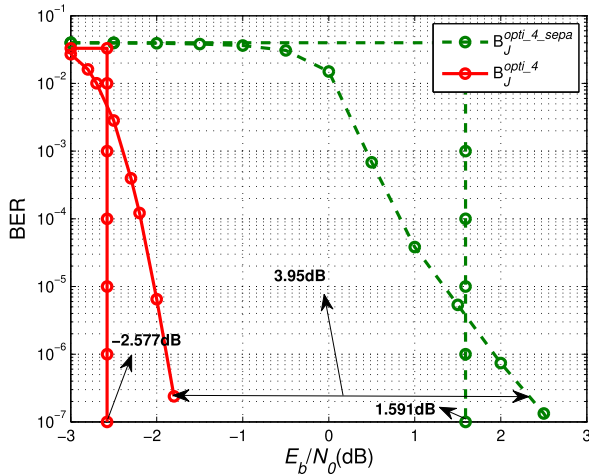


Fig. 11. BER simulation results of the JSCC system based on the proposed joint design and optimization algorithm and its separation-based counterpart at $N = 12800$.

TABLE III

DECODING THRESHOLDS OF THE JOINT BASE MATRICES APPLIED TO THE JSCC SYSTEM AND ITS SEPARATION-BASED COUNTERPART

Equation	JSCC system	separation-based system
$\mathbf{B}_J^{opti_1}$	-2.288 dB	0.462 dB
$\mathbf{B}_J^{opti_2}$	-2.388 dB	1.316 dB
$\mathbf{B}_J^{opti_3}$	-2.276 dB	0.551 dB
$\mathbf{B}_J^{opti_4}$	-2.577 dB	1.591 dB

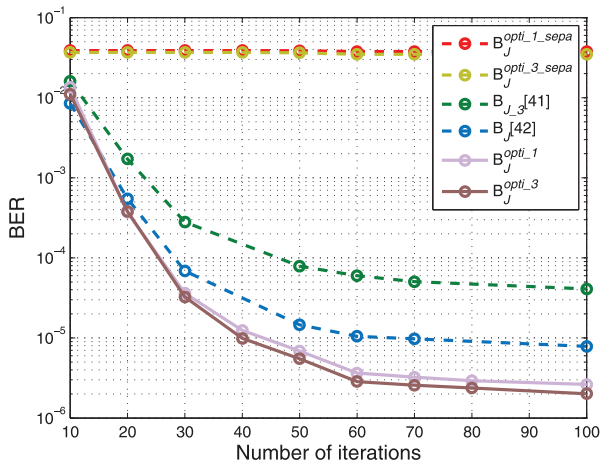


Fig. 12. The relationship between the number of iterations and the BER performance of the codes based on the proposed joint design and optimization algorithm and the codes in [41] and [42] for $N = 3200$, $E_b/N_0 = -0.8$ dB.

that $\mathbf{B}_J^{opti_1}$, $\mathbf{B}_J^{opti_2}$, $\mathbf{B}_J^{opti_3}$ and $\mathbf{B}_J^{opti_4}$ have 2.25 dB, 3.65 dB, 2.95 dB and 3.95 dB performance gains compared with $\mathbf{B}_J^{opti_1_sepa}$, $\mathbf{B}_J^{opti_2_sepa}$, $\mathbf{B}_J^{opti_3_sepa}$ and $\mathbf{B}_J^{opti_4_sepa}$, respectively. This clearly shows the advantage of JSCC, which can be attributed to the fact that the JSC decoder can effectively exploit source redundancy in the decoding process.

It can also be seen that the simulation results are consistent with the JPEXIT analyses (see Table I ~ Table III). One can readily conclude that the new design enables the system to

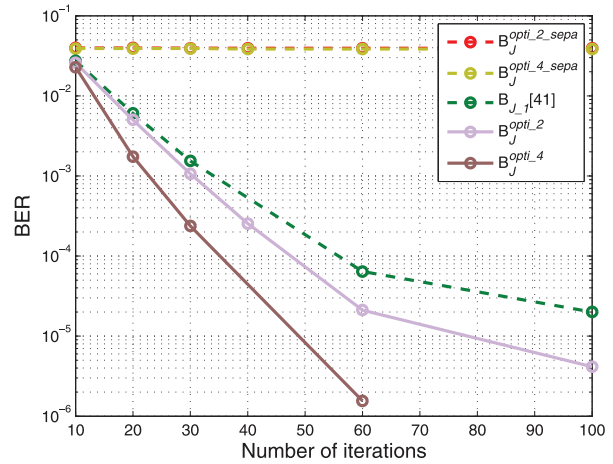


Fig. 13. The relationship between the number of iterations and the BER performance of the codes based on the proposed joint design and optimization algorithm and the code in [41] for $N = 12800$, $E_b/N_0 = -1.8$ dB.

reach the target BER at a lower SNR, thus improves the energy efficiency.

Moreover, compared with the previous designs, the base matrices constructed in the present work have smaller size and element value, thus are more desirable in terms of search and computational complexities. Fig. 12 and Fig. 13 illustrate the relationship between the number of iterations and the BER performance. It can be found that for the same target BER, the codes designed in this paper require fewer iterations. This observed acceleration of convergence is a result of good code structures, and is highly preferable for low-latency communications.

V. CONCLUSION

We have proposed an optimization algorithm based on the idea of MODE for the joint component design of the joint base matrix \mathbf{B}_J . The proposed algorithm takes into account various influencing factors in system design, such as source statistics, code rate, code length, row weight, column weight, and even the range of specific element value of the code.

The main results of this paper are summarized as follows. Firstly, regardless whether or not \mathbf{B}_{L2} is zero, a better joint basis matrix is designed under the unrelaxed conditions (suitable for short code design) and the relaxed conditions (suitable for long code design); significant performance gains are achieved as compared with the previously designed codes. Secondly, taking the joint decoding threshold $Th(\mathbf{B}_J)$ and the source threshold $STh(\mathbf{B}_J)$ as the optimization objectives, the joint base matrices designed in our work are able to reach lower decoding thresholds, that is, to achieve the waterfall performance, while avoiding the appearance of higher error floors. Our JSCC system also shows significant performance improvement over its separation-based counterpart. Finally, compared with the previous designs, the base matrices in this work have smaller size and element value, leading to lower search and computational complexities; the reduced number of iterations and the acceleration of convergence also makes the overall encoding/decoding process more efficient.

The systematic design and optimization approach proposed in this work effectively bridges the gap between theoretical analyses and practical implementations. It has the potential to expedite the adoption of the JSCC technology. We envision that the proposed approach can be further improved by leveraging advanced learning techniques. Exploring this research direction is an endeavor well worth undertaking.

REFERENCES

- [1] Y. Zhong, F. Alajaji, and L. L. Campbell, "On the joint source-channel coding error exponent for discrete memoryless systems," *IEEE Trans. Inf. Theory*, vol. 52, no. 4, pp. 1450–1468, Apr. 2006.
- [2] X. Chen, "Zero-delay Gaussian joint source–channel coding for the interference channel," *IEEE Commun. Lett.*, vol. 22, no. 4, pp. 712–715, Apr. 2018.
- [3] O. Fresnedo, P. Suarez-Casal, and L. Castedo, "Transmission of spatio-temporal correlated sources over fading multiple access channels with DQLC mappings," *IEEE Trans. Commun.*, vol. 67, no. 8, pp. 5604–5617, Aug. 2019.
- [4] S. Deka and K. K. Sarma, "Joint source channel coding with MIMO MC-CDMA for efficient communication," in *Proc. 2nd Int. Conf. Innov. Electron., Signal Process. Commun. (IESC)*, Mar. 2019, pp. 60–65.
- [5] J. Modestino and D. Daut, "Combined source-channel coding of images," *IEEE Trans. Commun.*, vol. 27, no. 11, pp. 1644–1659, Nov. 1979.
- [6] M. van der Schaar, S. Krishnamachari, S. Choi, and X. Xu, "Adaptive cross-layer protection strategies for robust scalable video transmission over 802.11 w lans," *IEEE J. Sel. Areas Commun.*, vol. 21, no. 10, pp. 1752–1763, Dec. 2003.
- [7] C. Y. Bi and J. Liang, "Joint source-channel coding of jpeg 2000 image transmission over two-way multi-relay networks," *IEEE Trans. Image Process.*, vol. 26, no. 7, pp. 3594–3608, Jul. 2017.
- [8] M. Martini, M. Mazzotti, C. Lamy-Bergot, J. Huusko, and P. Amon, "Content adaptive network aware joint optimization of wireless video transmission," *IEEE Commun. Mag.*, vol. 45, no. 1, pp. 84–90, Jan. 2007.
- [9] E. Bourtsoulatzé, D. Burth Kurka, and D. Gunduz, "Deep joint source-channel coding for wireless image transmission," *IEEE Trans. Cognit. Commun. Netw.*, vol. 5, no. 3, pp. 567–579, Sep. 2019.
- [10] M. Hassanin and J. Garcia-Frias, "Analog mappings for non-linear channels with applications to underwater channels," *IEEE Trans. Commun.*, vol. 68, no. 1, pp. 445–455, Jan. 2020.
- [11] R. G. Gallager, *Low Density Parity Check Codes*. Cambridge, MA, USA: MIT Press, 1963.
- [12] R. Tanner, "A recursive approach to low complexity codes," *IEEE Trans. Inf. Theory*, vol. 27, no. 5, pp. 533–547, Sep. 1981.
- [13] J. Thorpe, "Low-density parity-check (LDPC) codes constructed from protographs," *IPN Prog. Rep.*, vol. 42, pp. 42–154, Aug. 2003.
- [14] D. Divsalar, S. Dolinar, C. R. Jones, and K. Andrews, "Capacity-approaching protograph codes," *IEEE J. Sel. Areas Commun.*, vol. 27, no. 6, pp. 876–888, Aug. 2009.
- [15] A. Abbasfar, D. Divsalar, and K. Yao, "Accumulate-repeat-accumulate codes," *IEEE Trans. Commun.*, vol. 55, no. 4, pp. 692–702, Apr. 2007.
- [16] T. Richardson, "Multi-edge type LDPC codes," in *Proc. Workshop Honoring Prof. Bob McEliece 60th Birthday*, California Institute of Technology, Pasadena, CA, USA, May 2002, pp. 24–25.
- [17] D. Divsalar, S. Dolinar, and J. Thorpe, "Accumulate-repeat-accumulate-codes," in *Proc. IEEE 60th Veh. Technol. Conf. (VTC-Fall)*, Los Angeles, CA, USA, Sep. 2004, pp. 2292–2296.
- [18] D. Divsalar, S. Dolinar, and C. Jones, "Low-rate LDPC codes with simple protograph structure," in *Proc. Int. Symp. Inf. Theory (ISIT)*, Adelaide, SA, Australia, 2005, pp. 1622–1626.
- [19] D. Divsalar, C. Jones, S. Dolinar, and J. Thorpe, "Protograph based LDPC codes with minimum distance linearly growing with block size," in *Proc. IEEE Global Telecommun. Conf. (GLOBECOM)*, St. Louis, MO, USA, 2005, pp. 1152–1156.
- [20] T. V. Nguyen, A. Nosratinia, and D. Divsalar, "The design of rate-compatible protograph LDPC codes," *IEEE Trans. Commun.*, vol. 60, no. 10, pp. 2841–2850, Oct. 2012.
- [21] T. V. Nguyen and A. Nosratinia, "Rate-compatible short-length protograph LDPC codes," *IEEE Commun. Lett.*, vol. 17, no. 5, pp. 948–951, May 2013.
- [22] T. Van Nguyen, A. Nosratinia, and D. Divsalar, "Rate-compatible protograph-based LDPC codes for inter-symbol interference channels," *IEEE Commun. Lett.*, vol. 17, no. 8, pp. 1632–1635, Aug. 2013.
- [23] H. Uchikawa, "Design of non-precoded protograph-based LDPC codes," in *Proc. IEEE Int. Symp. Inf. Theory*, Honolulu, HI, USA, Jun. 2014, pp. 2779–2783.
- [24] A. K. Pradhan, A. Thangaraj, and A. Subramanian, "Construction of near-capacity protograph LDPC code sequences with block-error thresholds," *IEEE Trans. Commun.*, vol. 64, no. 1, pp. 27–37, Jan. 2016.
- [25] Y. Fang, P. Chen, L. Wang, and F. C. M. Lau, "Design of protograph LDPC codes for partial response channels," *IEEE Trans. Commun.*, vol. 60, no. 10, pp. 2809–2819, Oct. 2012.
- [26] P. Chen, K. Cai, and S. Zheng, "Rate-adaptive protograph LDPC codes for multi-level-cell NAND flash memory," *IEEE Commun. Lett.*, vol. 22, no. 6, pp. 1112–1115, Jun. 2018.
- [27] Y. He, M. Jiang, X. Ling, and C. Zhao, "Protograph-based EXIT analysis and optimization of LDPC coded DCO-OFDM in VLC systems," *IEEE Photon. Technol. Lett.*, vol. 30, no. 21, pp. 1898–1901, Nov. 1, 2018.
- [28] D. J. C. MacKay and R. M. Neal, "Near Shannon limit performance of low-density parity-check codes," *Electron. Lett.*, vol. 33, no. 6, pp. 457–458, Mar. 1997.
- [29] M. Fresia, F. Perez-Cruz, H. V. Poor, and S. Verdú, "Joint source and channel coding," *IEEE Signal Process. Mag.*, vol. 27, no. 6, pp. 104–113, Nov. 2010.
- [30] J. He, L. Wang, and P. Chen, "A joint source and channel coding scheme based on simple protograph structured codes," in *Proc. Int. Symp. Commun. Inf. Technol. (ISCIT)*, Gold Coast, QLD, Australia, Oct. 2012, pp. 65–69.
- [31] L. Wang, H. Wu, and S. Hong, "The sensitivity of joint source-channel coding based on double protograph LDPC codes to source statistics," in *Proc. 9th Int. Symp. Med. Inf. Commun. Technol. (ISMICT)*, Kamakura, Japan, Mar. 2015, pp. 24–26.
- [32] H. Wu, L. Wang, S. Hong, and J. He, "Performance of joint source-channel coding based on protograph LDPC codes over Rayleigh fading channels," *IEEE Commun. Lett.*, vol. 18, no. 4, pp. 652–655, Apr. 2014.
- [33] C. Chen, L. Wang, and Z. Xiong, "Matching criterion between source statistics and source coding rate," *IEEE Commun. Lett.*, vol. 19, no. 9, pp. 1504–1507, Sep. 2015.
- [34] Q. Chen, L. Wang, S. Hong, and Z. Xiong, "Performance improvement of JSCC scheme through redesigning channel code," *IEEE Commun. Lett.*, vol. 20, no. 6, pp. 1088–1091, Jun. 2016.
- [35] C. Chen, L. Wang, and S. Liu, "The design of protograph LDPC codes as source codes in a JSCC system," *IEEE Commun. Lett.*, vol. 22, no. 4, pp. 672–675, Apr. 2018.
- [36] H. V. Beltral Neto and W. Henkel, "Multi-edge optimization of low-density parity-check codes of joint source-channel coding," in *Proc. 9th Int. ITG Conf. Syst., Commun. Coding (SCC)*, Munich, Germany, Jan. 2013, pp. 1–6.
- [37] S. Hong, Q. Chen, and L. Wang, "Performance analysis and optimisation for edge connection of JSCC system based on double protograph LDPC codes," *IET Commun.*, vol. 12, no. 2, pp. 214–219, Jan. 2018.
- [38] S. Liu, C. Chen, L. Wang, and S. Hong, "Edge connection optimization for JSCC system based on DP-LDPC codes," *IEEE Wireless Commun. Lett.*, vol. 8, no. 4, pp. 996–999, Aug. 2019.
- [39] L. Xu, L. Wang, S. Hong, and H. Wu, "New results on radiography image transmission with unequal error protection using protograph double LDPC codes," in *Proc. 8th Int. Symp. Med. Inf. Commun. Technol. (ISMICT)*, Florence, Italy, Apr. 2014, pp. 1–4.
- [40] L. Deng, Z. Shi, O. Li, and J. Ji, "Joint coding and adaptive image transmission scheme based on DP-LDPC codes for IoT scenarios," *IEEE Access*, vol. 7, pp. 18437–18449, 2019.
- [41] C. Chen, L. Wang, and F. C. M. Lau, "Joint optimization of protograph LDPC code pair for joint source and channel coding," *IEEE Trans. Commun.*, vol. 66, no. 8, pp. 3255–3267, Aug. 2018.
- [42] Q. Chen, L. Wang, S. Hong, and Y. Chen, "Integrated design of JSCC scheme based on double protograph LDPC codes system," *IEEE Commun. Lett.*, vol. 23, no. 2, pp. 218–221, Feb. 2019.
- [43] X. Chen, W. Du, and F. Qian, "Multi-objective differential evolution with ranking-based mutation operator and its application in chemical process optimization," *Chemometric Intell. Lab. Syst.*, vol. 136, pp. 85–96, Aug. 2014.
- [44] X.-Y. Hu, E. Eleftheriou, and D. M. Arnold, "Regular and irregular progressive edge-growth tanner graphs," *IEEE Trans. Inf. Theory*, vol. 51, no. 1, pp. 386–398, Jan. 2005.
- [45] R. Storm and K. Price, "Differential evolution—a simple and efficient heuristic for global optimization over continuous spaces," *J. Global Optim.*, vol. 11, no. 4, pp. 341–359, 1997.



Sanya Liu received the B.S. degree in communication engineering from Binzhou University, Binzhou, China, in 2011, and the M.S. degree in electronics and communication engineering from Ningxia University, Ningxia, China, in 2014. She is currently pursuing the Ph.D. degree with the Department of Information and Communication Engineering, Xiamen University, Xiamen, China.

She is currently a Visiting Student with the Department of Electrical and Computer Engineering, McMaster University, Hamilton, ON, Canada.

Her current research interests include information theory, source coding, joint source and channel coding and their applications to wireless communication, and image processing.

Ms. Liu is currently an Invited Reviewer of IEEE TRANSACTIONS ON COMMUNICATIONS and IEEE TRANSACTIONS ON VEHICULAR TECHNOLOGY.



Lin Wang (Senior Member, IEEE) received the Ph.D. degree in electronics engineering from the University of Electronic Science and Technology of China, Chengdu, China, in 2001. From 1984 to 1986, he was a Teaching Assistant with the Mathematics Department, Chongqing Normal University. From 1989 to 2002, he was a Teaching Assistant, a Lecturer, and then an Associate Professor of applied mathematics and communication engineering with the Chongqing University of Posts and Telecommunications, China. From 1995 to 1996,

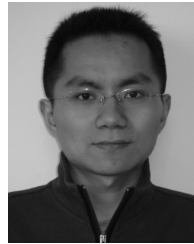
he spent one year with the Mathematics Department, University of New England, Australia. In 2003, he spent three months as a Visiting Researcher with the Center for Chaos and Complexity, Department of Electronic Engineering, City University of Hong Kong. In 2013, he was a Senior Visiting Researcher with the Department of ECE, UC Davis. He was a Distinguished Professor with Xiamen University, China, from 2012 to 2017, where he has been a Full Professor with the School of Informatics since 2003. He has authored more than 190 journal and conference papers (including 58 IEEE journal articles). He holds 21 patents in physical layer in digital communications. His current research interests include source coding/channel coding, joint source and channel coding/decoding, chaos modulation and their applications to wired/wireless communication, and underwater acoustic communications.



Jun Chen (Senior Member, IEEE) received the B.E. degree in communication engineering from Shanghai Jiao Tong University, Shanghai, China, in 2001, and the M.S. and Ph.D. degrees in electrical and computer engineering from Cornell University, Ithaca, NY, USA, in 2004 and 2006, respectively.

He was a Post-Doctoral Research Associate with the Coordinated Science Laboratory, University of Illinois at Urbana-Champaign, Urbana, IL, USA, from September 2005 to July 2006, and a Post-Doctoral Fellow at the IBM Thomas J. Watson Research Center, Yorktown Heights, NY, USA, from July 2006 to August 2007. Since September 2007, he has been with the Department of Electrical and Computer Engineering, McMaster University, Hamilton, ON, Canada, where he is currently a Professor. His research interests include information theory, machine learning, wireless communications, and signal processing.

Dr. Chen was a recipient of the Josef Raviv Memorial Postdoctoral Fellowship in 2006, the Early Researcher Award from the Province of Ontario in 2010, the IBM Faculty Award in 2010, the JSPS Invitational Fellowship in 2020, and the ICC Best Paper Award in 2020. He held the title of the Barber-Gennum Chair in Information Technology from 2008 to 2013 and the Joseph Ip Distinguished Engineering Fellow from 2016 to 2018. He served as an Associate Editor for IEEE TRANSACTIONS ON INFORMATION THEORY from 2014 to 2016. He is currently an Editor of IEEE TRANSACTIONS ON GREEN COMMUNICATIONS AND NETWORKING.



Shaohua Hong (Member, IEEE) received the B.S. degree in electronics and information engineering and the Ph.D. degree in electronics science and technology from Zhejiang University, Hangzhou, China, in 2005 and 2010, respectively.

He is currently an Associate Professor with the Department of Information and Communication Engineering, Xiamen University, Xiamen, China. His research interests include joint source and channel coding, wireless communication, and image processing.

Dr. Hong has been serving as an Editor for *KSII Transactions on Internet and Information Systems* since 2015.